DOI: 10.1002/chem.200700612

Giant Polyniobate Clusters Based on $[Nb_7O_{22}]^{9-}$ Units Derived from a Nb_6O_{19} Precursor

Jingyang Niu,[a] Pengtao Ma,[a] Hongyu Niu,[a] Jie Li,[a] Junwei Zhao,[b] You Song,[c] and Jingping Wang*[a]

Abstract: Rational self-assembly of hexaniobate Lindqvist-type precursor $[HNb_6O_{19}]^{7-}$ with soluble Cu^{2+} salts utilizing different strategies produces a series of giant polyniobate clusters, namely, $(H_2en)_{1.25}[Cu(en)_2(H_2O)]_2$-$Cl_4[Nb_{24}O_{72}H_{21.5}]\cdot 7H_2O$ (**1**; en: ethylenediamine), $[Cu(en)_2]_3[Cu(en)_2(H_2O)]_9$-$[\{H_2Nb_6O_{19}\}\subset\{[(\{KNb_{24}O_{72}H_{10.25}\}\{Cu$-$(en)_2\})_2\{Cu_3(en)_3(H_2O)_3\}\{Na_{1.5}Cu_{1.5}$-$(H_2O)_8\}\{Cu(en)_2\}_4]_6\}]\cdot 144H_2O$ (**2**), $K_{12}Na_4[H_{23}NaO_8Cu_{24}(Nb_7O_{22})_8]\cdot 106H_2O$ (**3**), and $K_{16}Na_{12}[H_9Cu_{25.5}O_8(Nb_7O_{22})_8]\cdot 73.5H_2O$ (**4**). Their structures were determined and further characterized by single-crystal X-ray diffraction analysis, IR and Raman spectroscopy, thermogravimetric analysis (TGA), and elemental analysis. Structural analyses reveal that compound **2** comprises a giant capsule anion based on a wheel-shaped cluster encapsulating a Lindqvist diprotonated cluster $[H_2Nb_6O_{19}]^{6-}$ unit, and forms a honeycomb-like structure with the inclusion of Lindqvist-type anions $[H_2Nb_6O_{19}]^{6-}$ in the holes, whereas **3** and **4** represent an unprecedented giant cube-shaped framework. All the compounds are built from $[Nb_7O_{22}]^{9-}$ fundamental building blocks. Solution Raman spectroscopy studies of **2** and **3** reveal that the solid-state structures of these polyniobate cluster anions disassemble and exist in the form of the $[Nb_6O_{19}]^{8-}$ unit in solution. Magnetic susceptibility measurement of **3** shows antiferromagnetic coupling interactions between Cu^{II} ions with the spin-canting phenomenon.

Keywords: cluster compounds · magnetic properties · niobium · polyoxometalates · self-assembly

Introduction

The ongoing search and exploration for novel polyoxometalate constructions are predominantly driven by their fascinating properties and manifold potential applications in such fields as catalysis, medicine, and materials science, as well as their intriguing topological structures.[1–6] However, to date, the development of polyoxometalate chemistry is still dominated by those of the elements W, Mo, and V, because their polyanions can be easily formed over a wide pH range and sometimes can be produced simply by acidification and fusion of their oxoanion solutions at standard pressure and ambient temperature. For example, in 1997, a giant polyanion containing 148 tungsten atoms, $[As_{12}Ce_{16}$-$(H_2O)_{36}W_{148}O_{524}]^{76-}$, was reported by the Pope group.[7] Another large wheel-shaped Cu_{20} cluster incorporating the tungstophosphate $[Cu_{20}Cl(OH)_{24}(H_2O)_{12}(P_8W_{48}O_{184})]^{25-}$ ion was also depicted by Kortz et al. in 2005.[8] However, under similar conditions, these oxoanion precursors in Nb and Nb-oxo chemistry are not available and are mainly dominated by the Lindqvist-type anion $[Nb_6O_{19}]^{8-}$.[9] Although hexaniobates, one of which was first structurally characterized in 1980 as a monoprotonated cluster $[HNb_6O_{19}]^{7-}$,[10] act as a cornerstone for the advancement of polyoxoniobate chemistry, they are very stable and possess lower reaction activity with paramagnetic transition-metal cations or transition-

[a] Prof. Dr. J. Niu, P. Ma, H. Niu, J. Li, Prof. Dr. J. Wang
Institute of Molecular and Crystal Engineering
School of Chemistry and Chemical Engineering
Henan University
Minglun Street 85, Kaifeng 475001 (China)
Fax: (+86) 378 2865 974
E-mail: jpwang@henu.edu.cn

[b] Dr. J. Zhao
State Key Laboratory of Structural Chemistry
Fujian Institute of Research on the Structure of Matter
Chinese Academy of Sciences
Fuzhou, Fujian 350002 (China)

[c] Prof. Dr. Y. Song
State Key Laboratory of Coordination Chemistry
Nanjing University
Nanjing 210093 (China)

Supporting information for this article is available on the WWW under http://www.chemeurj.org/ or from the author.

metal complexes, directly resulting in the slow evolution of the polyoxoniobate chemistry.[9] Presently, the most useful synthetic procedures for polyniobates are by means of the freshly precipitated hydrated oxide, based on direct dissolution of Nb_2O_5 in aqueous alkali or fusion of Nb_2O_5 with excess metal hydroxide or carbonate.[11] To dissolve these Nb precursors by using "beaker chemistry", many excess equivalents of base are required. Nevertheless, as the concentration of AOH (A: alkali-metal ion) increases in solution, the Lindqvist-type compound $A_8[Nb_6O_{19}]$ is salted out as a major product. Therefore, to form other polyniobate clusters, it is necessary to find appropriate conditions in which the Nb precursors are dissolved. Graeber and Morosin utilized a nonaqueous solvent to produce an isodecaniobate, $[Nb_{10}O_{28}]^{6-}$, under ambient conditions.[12] Nyman and co-workers reported two types of heteropolyniobates, $[XNb_{12}O_{40}]^{16-}$ (X: Si^{IV} or Ge^{IV}) and $[H_2Si_4Nb_{16}O_{56}]^{14-}$, in hydrothermal environments.[13] Recently, Nyman et al. again reported a novel lacunary heteropolyniobate $[(PO_2)_3PNb_9O_{34}]^{15-}$[14] and a large isopolyniobate cluster $\{Nb_{24}O_{72}H_9\}^{15-}$[15] by routine aqueous solution methods. Moreover, Yagasaki et al. obtained a dimeric isopolyanion $[Nb_{20}O_{54}]^{8-}$.[16] Although polyniobate chemistry has made progress to some extent in the preparation and characterization of some novel compounds, the systematic synthesis and property investigation of these systems remain less developed. Furthermore, the polyniobate family attracts perpetual interest for a vast range of potential applications in virology,[3c] nuclear-waste treatment,[9g,23a] and the base-catalyzed decomposition of biocontaminants,[17b] resulting from their unique characteristics in structure (high charge/surface ratio) and properties (basicity).

To extend and explore polyniobate clusters as anionic ligands to coordinate transition metals and, further, give rise to much larger polyniobate aggregates or multidimensional polyniobate architectures, we developed an effective strategy in which hexaniobates can be used as precursors to synthesize other polyniobates and sometimes as intermediates to construct other polyniobate topologies. In the course of our ongoing investigation on the formation and construction of the large Nb-oxo clusters based on the Lindqvist-type anion $[Nb_6O_{19}]^{8-}$ and transition-metal ions, a series of new polyniobate clusters has been obtained in aqueous solution. Among them, the polyniobate cluster $(H_2en)_{1.25}[Cu(en)_2(H_2O)]_2Cl_4[Nb_{24}O_{72}H_{21.5}]\cdot 7H_2O$ (**1**) (en: ethylenediamine) utilizes the same structure type reported recently by Nyman et al. (see the Supporting Information).[14] Most importantly, three new polyniobates, $[Cu(en)_2]_3[Cu(en)_2(H_2O)]_9[\{H_2Nb_6O_{19}\}\subset\{[(\{KNb_{24}O_{72}H_{10.25}\}\{Cu(en)_2\})_2\{Cu_3(en)_3(H_2O)_3\}\{Na_{1.5}Cu_{1.5}(H_2O)_8\}\{Cu(en)_2\}_4]_6\}]\cdot 144H_2O$ (**2**), $K_{12}Na_4[H_{23}NaO_8Cu_{24}(Nb_7O_{22})_8]\cdot 106H_2O$ (**3**), and $K_{16}Na_{12}[H_9Cu_{25.5}O_8(Nb_7O_{22})_8]\cdot 73.5H_2O$ (**4**), were obtained by distinct synthetic methods in the basic region (pH 10–11), which are of great significance to the extensive research of polyniobate chemistry and also provide a comparatively systematic method for the exploration of other transition-metal polyniobate derivatives.

Results and Discussion

Syntheses: Based on the previous work, we further explored the synthetic strategy of polyniobates. In the syntheses of compounds **1** and **2**, ethylenediamine (en) was chosen as the ligand according to two considerations: 1) it can interact with copper(II) acetate (Ac), first leading to the complex $Cu(en)_2(Ac)_2$, which can stably exist in the system of hexaniobate and 2) it can also be used to adjust the pH value of the solution. As we know, many factors (reactants, temperature and time of reaction, pH value, and concentration of reaction system) can influence the structures and extended structural fashions of products. As for the syntheses of **1** and **2**, temperature and time of reaction play the most important roles, but for **3** and **4** the reactants are more important. During the synthetic processes of **3** and **4**, silver nitrate ($AgNO_3$) for **3** and barium chloride ($BaCl_2$) for **4** act as precipitators, which first react with hexaniobate resulting in a white precipitate, and then react with $CuCl_2$ or $CuSO_4$ leading to the products. The possible formation mechanism is that the precipitator $AgNO_3$ or $BaCl_2$ can partially precipitate $Na_7HNb_6O_{19}\cdot 15H_2O$ and $K_7HNb_6O_{19}\cdot 13H_2O$ by the formation of the possible $Ag_xNa_{7-x}HNb_6O_{19}\cdot nH_2O$ or $Ba_xK_{7-2x}HNb_6O_{19}\cdot nH_2O$ precipitates, and then compounds **3** and **4** form upon addition of $CuCl_2\cdot 2H_2O$ or $CuSO_4\cdot 5H_2O$. The use of this strategy introduces copper ions into the niobium-oxo units, while silver and barium ions are isolated by the formation of silver chloride and barium sulfate. In contrast, by removing $AgNO_3$ or $BaCl_2\cdot 2H_2O$ in the preparation procedures, compounds **3** and **4** cannot be formed. Therefore, $AgNO_3$ and $BaCl_2\cdot 2H_2O$ play a crucial role in the production of **3** and **4**. However, the specific roles of $AgNO_3$ and $BaCl_2\cdot 2H_2O$ in the preparation of **3** and **4** are not well understood; in the upcoming exploration, we will continue to probe and investigate the formation mechanism and the pertinent synthetic chemistry. Moreover, the exploration of hexaniobate precursors as basic inorganic building blocks to accommodate other transition-metal or rare-earth cations is in progress.

Structure: The fundamental building block $[Nb_7O_{22}]^{9-}$ (see Figure S1 in the Supporting Information) in **1**–**4** is derived from the Lindqvist-type hexaniobate anion $[Nb_6O_{19}]^{8-}$, the three adjacent μ_2-oxygen atoms of which are combined with the seventh Nb atom, Nb(7). More interestingly, the $Nb(7)O_6$ octahedron in the $[Nb_7O_{22}]^{9-}$ fragment has three terminal oxygen atoms with higher coordination ability than the other six NbO_6 octahedra, which provides an inevitable condition for the structural architectures of compounds **1**–**4** (Table 1).

As in the description of Nyman, the very high number of crystallographically independent atoms and variable parameters prevented the direct location of the protons from the Fourier maps; even bond-valence calculations did not provide an obvious solution as a result of atypical distortions and the relatively wide variation of the Nb–O bond lengths.[15] In the structures of the $\{Nb_{24}O_{72}\}$ and $\{KNb_{24}O_{72}\}$

Table 1. Crystallographic data structure refinement for compounds **1**–**4**.

	1	**2**	**3**	**4**
Formula	$C_{21}H_{168}C_{18}Cu_4N_{21}Nb_{48}O_{162}$	$C_{114}H_{737.5}Cu_{37.5}K_6N_{114}Na_{4.5}Nb_{147}O_{551}$	$H_{235}Cu_{24}K_{12}Na_5Nb_{56}O_{290}$	$H_{156}Cu_{25.5}K_{16}Na_{12}Nb_{56}O_{257.5}$
M_r [g mol^{-1}]	8304.91	28 904.26	12 188.95	12 001.96
crystal system	triclinic	hexagonal	triclinic	triclinic
space group	$P\bar{1}$	$R3c$	$P\bar{1}$	$P\bar{1}$
crystal size [mm]	0.21×0.17×0.13	0.26×0.25×0.19	0.26×0.18×0.13	0.18×0.16×0.13
a [Å]	16.182(3)	63.104(3)	20.523	19.194(4)
b [Å]	23.808(5)	63.104(3)	21.049(4)	20.962(4)
c [Å]	24.472(5)	47.729(3)	21.254(4)	22.876(4)
α [°]	119.07(3)	90	108.49(3)	73.079(2)
β [°]	93.99(3)	90	94.50(3)	70.046(2)
γ [°]	91.80(3)	120	102.98(3)	88.281(3)
V [Å3]	8198(3)	164 599(15)	8373(3)	8252(3)
ρ_{calcd} [g cm^{-3}]	1.679	1.750	2.417	2.415
Z	1	6	1	1
μ [mm^{-1}]	1.991	2.276	3.582	3.776
limiting indices	$0 \le h \le 19$	$-75 \le h \le 75$	$0 \le h \le 24$	$-16 \le h \le 22$
	$-28 \le k \le 28$	$-75 \le k \le 74$	$-25 \le k \le 24$	$-22 \le k \le 24$
	$-29 \le l \le 28$	$-56 \le l \le 56$	$-25 \le l \le 25$	$-27 \le l \le 26$
reflns measured	23 973	369 832	18 955	38 862
independent reflns	23 973	30 224	18 955	27 324
observed reflns	14 938	17 390	16 094	18 204
parameters	1258	1706	1498	1496
R_1[a] [$I > 2\sigma(I)$]	0.0754	0.0494	0.0729	0.0717
wR_2[b] (all data)	0.2081	0.1310	0.1846	0.2023
largest diff. peak/hole [eÅ^{-3}]	2.828/−1.157	4.970/−1.467	4.940/−2.147	3.350/−1.998

[a] $R_1 = \Sigma ||F_o| - |F_c|| / \Sigma |F_c|$; [b] $wR_2 = \Sigma[w(F_o^2 - F_c^2)^2] / \Sigma[w(F_o^2)^2]^{1/2}$ with $1/w = \sigma^2 F_o^2 + aP^2 + bP$ and $P = F_o^2 + 2F_c^2/3$.

moieties in compounds **1** and **2**, three long Nb–O_t (t: terminal) bonds of the NbO_6 octahedra (shown in pink in Figures 1 and 2) linked to three $[Nb_7O_{22}]^{9-}$ building blocks are in the range of 2.347(8)–2.402(9) Å for **1** and 2.369(6)–2.421(6) Å for **2**, and bond valence sum (BVS)[18] calculations provided values of 0.265–0.308 (**1**) and 0.252–0.290 (**2**) for these Nb–O_t terminal oxygen atoms, indicating the most possible sites for protonation. The BVS values of the remaining terminal oxygen atoms in **1**–**4** are in the ranges of 1.15–1.60, 1.12–1.58, 1.21–1.58, and 1.24–1.56, respectively, suggesting that some terminal oxygen atoms can be monoprotonated. Although they cannot be accurately located by X-ray diffraction and BVS calculations, these protons must be localized or delocalized in polyniobate anion units. In addition, the terminal oxygen BVS values of 1.57 of the hexaniobate cluster unit included in **2** and the pH range of 10–11 in which the compound was obtained both suggest that the hexaniobate cluster anion is diprotonated $[H_2Nb_6O_{19}]^{6-}$. This result is in good agreement with previous studies, indicating that the diprotonated $[H_2Nb_6O_{19}]^{6-}$ anion predominates in solution in the pH range of 9–11.[19] Thus, these compounds are formulated as follows: $(H_2en)_{1.25}[Cu(en)_2(H_2O)]_2Cl_4[Nb_{24}O_{72}H_{21.5}]\cdot 7H_2O$ (**1**), $[Cu(en)_2]_3[Cu(en)_2(H_2O)]_9[\{H_2Nb_6O_{19}\}\subset\{[(\{KNb_{24}O_{72}H_{10.25}\}\{Cu(en)_2\})_2\{Cu_3(en)_3(H_2O)_3\}\{Na_{1.5}Cu_{1.5}(H_2O)_8\}\{Cu(en)_2\}_4]_6\}]\cdot 144H_2O$ (**2**), $K_{12}Na_4[H_{23}NaO_8Cu_{24}(Nb_7O_{22})_8]\cdot 106H_2O$ (**3**), and $K_{16}Na_{12}[H_9Cu_{25.5}O_8(Nb_7O_{22})_8]\cdot 73.5H_2O$ (**4**).

The X-ray powder diffraction patterns of **2**–**4** are in good agreement with the simulated pattern from the single-crystal X-ray data for these compounds (see Figures S21–S23 in the Supporting Information). The results confirm that the bulk samples of these compounds are pure.

X-ray structural analysis of compound **1** reveals the presence of the giant isopolyanion cluster $\{Nb_{24}O_{72}\}$ (see Figure 1 and Figure S2 in the Supporting Information), which is derived from two fundamental building blocks, namely, three $[Nb_7O_{22}]^{9-}$ cores and three NbO_6 octahedra, alternately linking into a discrete triangular "bowl-shaped" cluster structure approaching the C_{3v} point symmetry. Notably, the fundamental building block $[Nb_7O_{22}]^{9-}$ is derived from the Lindqvist-type hexaniobate anion $[Nb_6O_{19}]^{8-}$, the three adjacent μ_2-oxygen atoms of which are combined with the seventh Nb atom, Nb(7). To our knowledge, there is no analogous species reported in vanadium, molybdenum, and tungsten chemistry. The $[Nb_7O_{22}]^{9-}$ subunit has four types of O atoms (see Figure S1 in the Supporting Information): nine terminal oxygen atoms (O_t), nine bridging μ_2-oxygen atoms, three bridging μ_3-oxygen atoms, and one central μ_6-oxygen atom. The Nb–O_t, Nb–μ_2-O, Nb–μ_3-O, and Nb–μ_6-O bond lengths in **1** for three $[Nb_7O_{22}]^{9-}$ anions range from 1.737(10) to 1.860(9), from 1.876(9) to 2.077(10), from 2.028(8) to 2.280(7), and from 2.262(7) to 2.475(9) Å, respectively, and the Nb–Nb distances are in the range of 3.209(2) to 3.394(8) Å.

As shown in Figure 2, the fundamental building block of **2** is a dimeric fragment $[(\{KNb_{24}O_{72}H_{10.25}\}\{Cu(en)_2\})_2\{Cu_3(en)_3(H_2O)_3\}\{Na_{1.5}Cu_{1.5}(H_2O)_8\}]^{11-}$ constructed from two $[\{KNb_{24}O_{72}H_{10.25}\}\{Cu(en)_2\}]^{10.75-}$ moieties connected together by three disordered copper bridges (each copper site is shared by 50% Cu^{2+} and 50% Na^+ elements) and a tricop-

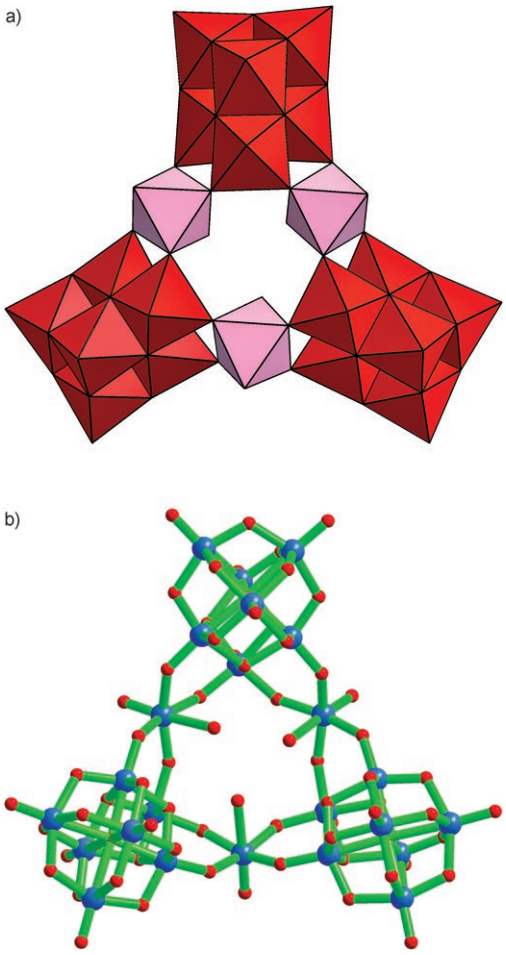

Figure 1. Polyhedral (a) and ball-and-stick (b) molecular structures of the polyanion $[Nb_{24}O_{72}H_{21.5}]^{2.5-}$ in **1**. The $[Nb_7O_{22}]^{9-}$ clusters in a) are shown as red polyhedra, whereas the bridging NbO_6 octahedra are shown as pink polyhedra.

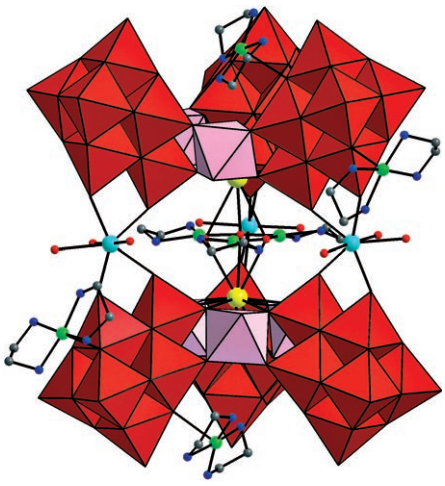

Figure 2. Combined polyhedral/ball-and-stick representation of the dimeric fundamental building block $[(\{KNb_{24}O_{72}H_{10.25}\}\{Cu(en)_2\})_2\{Cu_3(en)_3(H_2O)_3\}\{Na_{1.5}Cu_{1.5}(H_2O)_8\}]^{11-}$ in **2**. The $[Nb_7O_{22}]^{9-}$ units are red and the bridging NbO_6 octahedra are pink, while potassium, copper, oxygen, carbon, nitrogen, and disordered copper atoms are shown as yellow, green, red, light gray, blue, and cyan spheres, respectively.

per $\{Cu_3(en)_3(H_2O)_3\}^{6+}$ cluster bridge generating a novel sandwich-type structure. The $[KNb_{24}O_{72}H_{10.25}]^{12.75-}$ moiety (see Figure S4 in the Supporting Information) except for the "capped" K^+ ion in **2** is very similar to the giant isopolyanion $[Nb_{24}O_{72}H_{21.5}]^{2.5-}$ in **1**. The tricopper $\{Cu_3(en)_3(H_2O)_3\}^{6+}$ cluster consists of three four-coordinate $[Cu(en)]^{2+}$ cations linked to each other through three μ_4-H_2O bridges, and then coordinated to two K^+ cations from two $[KNb_{24}O_{72}H_{10.25}]^{12.75-}$ building blocks by means of the three μ_4-H_2O bridges (see Figures S5 and S6 in the Supporting Information). Compound **2** belongs to the hexagonal *R3c* space group, and thus the most intriguing structural feature is the gigantic inorganic–organic hybrid circle-shaped cavity structure built by six interconnecting $[(\{KNb_{24}O_{72}H_{10.25}\}\{Cu(en)_2\})_2\{Cu_3(en)_3(H_2O)_3\}\{Na_{1.5}Cu_{1.5}(H_2O)_8\}]^{11-}$ dimeric fragments through the six-coordinate $[Cu(en)_2]^{2+}$ linkages on the crystallographic *ab* plane (Figure 3). In the cavity surrounded by six interconnecting $[(\{KNb_{24}O_{72}H_{10.25}\}\{Cu(en)_2\})_2\{Cu_3(en)_3(H_2O)_3\}\{Na_{1.5}Cu_{1.5}$-

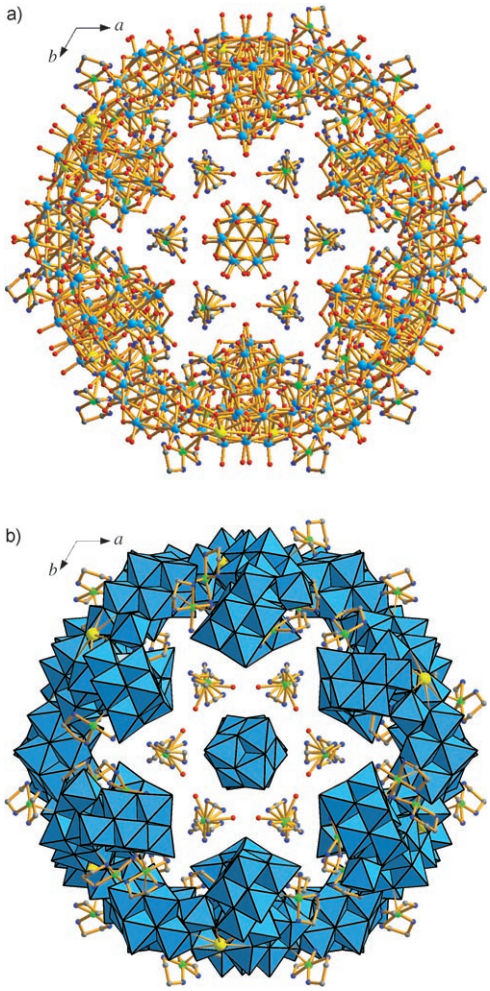

Figure 3. Ball-and-stick (a) and polyhedral (b) representation viewed down the crystallographic *c* axis of the construction motif of capsule anions $[\{H_2Nb_6O_{19}\}^{6-}[(\{KNb_{24}O_{72}H_{10.25}\}\{Cu(en)_2\})_2\{Cu_3(en)_3(H_2O)_3\}\{Na_{1.5}Cu_{1.5}(H_2O)_8\}\{Cu(en)_2\}_4]_6\}^{18-}]^{24-}$ in **2** via numerous $\{Cu(en)_2\}^{2+}$ bridges.

$(H_2O)_8\}]^{11-}$ dimeric fragments, a Lindqvist $[H_2Nb_6O_{19}]^{6-}$ anion and six five-coordinate $[Cu(en)_2(H_2O)]^{2+}$ cations are hosted (see Figure S7 in the Supporting Information). Most interestingly, each dimeric fragment $[(\{KNb_{24}O_{72}H_{10.25}\}\{Cu(en)_2\})_2\{Cu_3(en)_3(H_2O)_3\}\{Na_{1.5}Cu_{1.5}(H_2O)_8\}]^{11-}$ is combined with six of the same adjacent fragments to construct an unprecedented 3D, infinitely extended architecture (Figure 4).

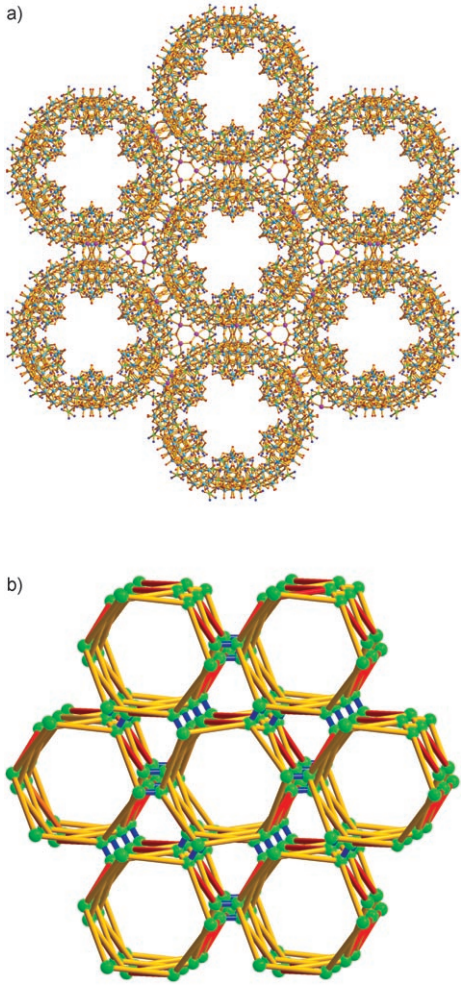

Figure 4. Ball-and-stick (a) and topology structure (b) of the 3D, infinitely extended, honeycomb-like configuration of **2** viewed down the *c* axis, which is built from capsule anions $[\{H_2Nb_6O_{19}\}^{6-}\subset[\{(\{KNb_{24}O_{72}H_{10.25}\}\{Cu(en)_2\})_2\{Cu_3(en)_3(H_2O)_3\}\{Na_{1.5}Cu_{1.5}(H_2O)_8\}\{Cu(en)_2\}_4\}_6\}^{18-}]^{24-}$ via numerous $\{Cu(en)_2\}^{2+}$ bridges. The green balls represent $[\{KNb_{24}O_{72}H_{10.25}\}\{Cu(en)_2\}]^{10.75-}$ building units; the light orange, red, and blue rods represent the single $\{Cu(en)_2\}^{2+}$ bridge, double $\{Cu(en)_2\}^{2+}$ bridge, and $\{Na_{1.5}Cu_{1.5}(H_2O)_8\}^{4.5+}$ bridges, respectively. Some discrete fragment ions and solvent molecules are omitted for clarity.

This architecture is built up by means of the connection motif of each dimeric fragment $[(\{KNb_{24}O_{72}H_{10.25}\}\{Cu(en)_2\})_2\{Cu_3(en)_3(H_2O)_3\}\{Na_{1.5}Cu_{1.5}(H_2O)_8\}]^{11-}$ with six of the same adjacent fragments. Specifically, each $[\{KNb_{24}O_{72}H_{10.25}\}\{Cu(en)_2\}]^{10.75-}$ unit is linked to three of the same clusters by four $\{Cu(en)_2\}^{2+}$ bridges through μ_3-O–Cu(en)$_2$–μ_3-O linkages (Cu–O: 2.561(6)–2.753(6) Å; see Table 2). However, each $[\{KNb_{24}O_{72}H_{10.25}\}\{Cu(en)_2\}]^{10.75-}$ unit is linked to three of the same adjacent clusters by two different modes: one mode is by a single $\{Cu(en)_2\}^{2+}$ bridge linking to an adjacent $[\{KNb_{24}O_{72}H_{10.25}\}\{Cu(en)_2\}]^{10.75-}$ unit through one μ_3-O–Cu(en)$_2$–μ_3-O linkage; the other is by two $\{Cu(en)_2\}^{2+}$ bridges linking to an adjacent $[\{KNb_{24}O_{72}H_{10.25}\}\{Cu(en)_2\}]^{10.75-}$ unit through two μ_3-O–Cu(en)$_2$–μ_3-O linkages (see Figures S8 and S9 in the Supporting Information). In addition, the closed wheel-shaped ring on the crystallographic *ab* plane can also be viewed as the packing distribution of six interconnecting $[\{KNb_{24}O_{72}H_{10.25}\}\{Cu(en)_2\}]^{10.75-}$ units by virtue of single $\{Cu(en)_2\}^{2+}$ bridges. Meanwhile, the two adjacent rings along the crystallographic *c* direction are interconnected by three double $\{Cu(en)_2\}^{2+}$ bridges, resulting in a snowflake-like tunnel along the crystallographic *c* axis with efficient inner and exterior diameters of 15.3 and 39.6 Å, respectively (see Figures S10 and S11 in the Supporting Information). Discrete Lindqvist-type polyanions $[H_2Nb_6O_{19}]^{6-}$ and complex cations $[Cu(en)_2(H_2O)]^{2+}$ reside in the tunnels to further stabilize the tunnel skeleton (Figure 3). Through the two above-mentioned construction motifs, an unprecedented 3D honeycomb-like configuration comes into being (see Figure 4 and Figure S12 in the Supporting Information). To the best of our knowledge, an example of such honeycomb-like polyniobate cluster anions with the inclusion of Lindqvist-type anions $[H_2Nb_6O_{19}]^{6-}$ in the tunnels has not been found hitherto.

X-ray diffraction of **3** indicates the formation of an unprecedented giant cube-shaped polyniobate cluster $\{NaO_8Cu_{24}(Nb_7O_{22})_8\}$ (see Figure 5 and Figures S13 and S14 in the Supporting Information) with an *O* point symmetry, which is composed of one NaO_8 cubelike unit acting as structure-directing motif, eight $[Nb_7O_{22}]^{9-}$ fundamental building blocks, and 24 Cu bridges. In the $\{NaO_8Cu_{24}(Nb_7O_{22})_8\}$ cluster, eight $[Nb_7O_{22}]^{9-}$ fundamental building blocks sit on the eight corner-sites of the cube. Every $[Nb_7O_{22}]^{9-}$ subunit donates six terminal oxygen atoms, three from the seventh NbO_6 octahedron and the others from neighboring different NbO_6 octahedra, then 24 Cu^{2+} cations bridge these 48 terminal oxygen atoms in a CuO_4 square-planar fashion (Cu–O: 1.889(8)–1.989(7) Å) forming a cubelike cavity occupied by the NaO_8 unit (Na–O: 2.341(8)–2.429(9) Å). In the direction of every edge of the NaO_8 cubelike unit, 12 such Cu_2O_2 units combine eight $[Nb_7O_{22}]^{9-}$ fundamental building blocks with the central NaO_8 cubelike unit via O–Cu–μ_2-O–Cu–O bridges (see Figure S15 in the Supporting Information).

Charge balance within the structure requires the presence of 23 protons per $\{NaO_8Cu_{24}(Nb_7O_{22})_8\}$ cluster unit, namely, $[H_{23}NaO_8Cu_{24}(Nb_7O_{22})_8]^{16-}$. In addition, to enhance the chemical stability of this giant cubelike cluster, six charge-compensation K^+ cations are facilitated to fill the six hydrophilic "tundish-shaped" cavities on the cubic side faces surrounded by the central Na^+ core and four adjacent $[Nb_7O_{22}]^{9-}$ fundamental building blocks. Clearly, all the

Table 2. Selected bond lengths [Å] of compound **2**.

Cu1–O4W#1	1.911(6)	Cu4–O9W#1	2.336(7)	Cu7–N12	2.037(11)
Cu1–O5W	1.912(2)	Cu4–O7A	2.344(6)	Cu7–O23#1	2.561(6)
Cu1–N1	1.981(7)	Cu4–O7A#1	2.344(6)	Cu7–O43	2.753(7)
Cu1–N2	1.996(7)	Cu5–N4	1.965(9)	Cu8–N16	2.005(19)
Cu2–O4W	1.937(6)	Cu5–N6	1.996(9)	Cu8–N16#2	2.005(19)
Cu2–O4W#1	1.937(6)	Cu5–N5	2.004(9)	Cu8–N17	2.037(16)
Cu2–N3#1	1.988(7)	Cu5–N7	2.018(8)	Cu8–N17#2	2.038(16)
Cu2–N3	1.988(7)	Cu5–O34	2.390(7)	Cu9–N20	1.977(12)
Cu3–O6W	2.340(7)	Cu6–N10	1.978(10)	Cu9–N18	1.999(13)
Cu3–O7W	2.361(8)	Cu6–N9	1.980(9)	Cu9–N19	2.001(16)
Cu3–O19	2.384(5)	Cu6–N11	1.996(9)	Cu9–N21	2.017(15)
Cu3–O9#1	2.438(6)	Cu6–N8	2.003(10)	Cu9–O10W	2.334(8)
Cu3–O14C#1	2.454(6)	Cu6–O28	2.640(6)	Cu10–N25	1.94(2)
Cu3–O21B	2.467(5)	Cu6–O49	2.661(7)	Cu10–N23	1.97(2)
Cu3–O8W	2.572(7)	Cu7–N15	1.965(11)	Cu10–N24	2.02(3)
Cu4–O6	2.325(6)	Cu7–N14	1.970(11)	Cu10–N22	2.11(2)
Cu4–O6#1	2.326(6)	Cu7–N13	1.972(10)	Cu10–O40	2.488(9)
Cu4–O9W	2.336(7)				

[a] Symmetry codes for compound **2**: #1 $y+1/3$, $x-1/3$, $-z+7/6$; #2 $x-y+2/3$, $-y+4/3$, $-z+11/6$.

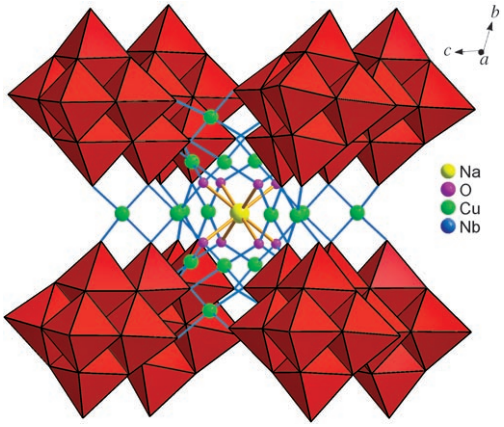

Figure 5. Combined polyhedral/ball-and-stick representation of the polyanion $[H_{23}NaO_8Cu_{24}(Nb_7O_{22})_8]^{16-}$ in **3**. The NbO_6 octahedra are shown in red; Cu, O, and Na atoms are shown as green, purple, and yellow spheres, respectively.

Cu^{2+} cations utilize the four-coordinate square-planar geometry rather than a six-coordinate octahedral configuration, mainly owing to the very large steric hindrance effects. From the above-mentioned structural analysis, the three terminal oxygen atoms from the seventh NbO_6 octahedron in the $[Nb_7O_{22}]^{9-}$ subunit and the square-planar bridging function of Cu^{2+} cations play an enormously important role in the formation and architecture of the $[H_{23}NaO_8Cu_{24}(Nb_7O_{22})_8]^{16-}$ cluster. In addition, the crystal structure of **3** shows that the macropolyniobate clusters $[H_{23}NaO_8Cu_{24}(Nb_7O_{22})_8]^{16-}$ lined up along the crystallographic *a* axis (see Figure 6 and Figure S16 in the Supporting Information) reveal one type of "elliptical" column, which are arranged to construct straight channels with sizes of 16×9 Å, whereas parallel to the crystallographic *c* axis they form two types of "hexagonal" and "S-shaped" columns with sizes of 18×10 and 15×10 Å, respectively.

Compound **4** reveals another giant cube-shaped polyniobate cluster $[H_9Cu_{25.5}O_8(Nb_7O_{22})_8]^{28-}$ (see Figure 7 and Figures S17 and S18 in the Supporting Information) with an *O* point symmetry, which is very similar to the construction motif of **3** except for the $Cu_{1.5}O_8$ core in place of the NaO_8 cubelike unit. In the $Cu_{1.5}O_8$ core, the Cu atoms are disordered in six positions, and the site occupancies of Cu13, Cu13A ($1-x$, $-y$, $1-z$), Cu14, Cu14A ($1-x$, $-y$, $1-z$), Cu15, and Cu15A ($1-x$, $-y$, $1-z$) atoms are 0.45, 0.45, 0.15, 0.15, 0.15, and 0.15, respectively. Therefore, there are 1.5 Cu atoms in the central

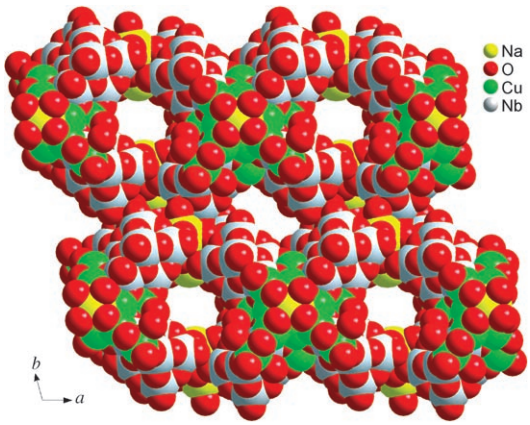

Figure 6. Space-filling packing of the polyanion $[H_{23}NaO_8Cu_{24}(Nb_7O_{22})_8]^{16-}$ in **3** viewed down the crystallographic *c* axis.

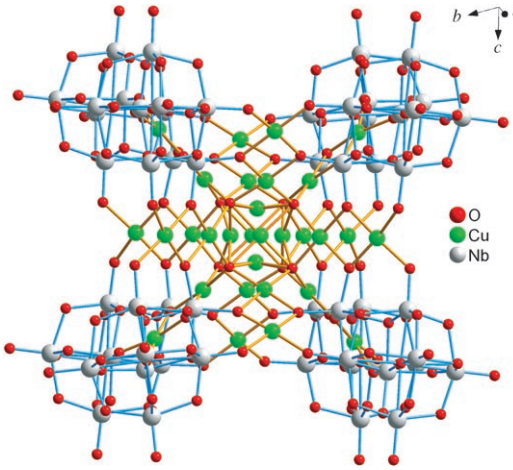

Figure 7. Ball-and-stick representation of the polyanion $[H_9Cu_{25.5}O_8(Nb_7O_{22})_8]^{28-}$ in **4**.

core. Moreover, the Cu13, Cu13A, Cu14, Cu14A, Cu15, and Cu15A atoms are respectively situated on the two corresponding face centers of the cube whose eight corner sites are made up of eight oxygen atoms.

IR and Raman spectra of compounds 1–4: IR studies of **2–4** show characteristic vibration patterns similar to those of a Lindqvist-type structure. In comparison with the IR spectrum of precursor $[HNb_6O_{19}]^{7-}$,[20,21] the characteristic bands corresponding to terminal Nb–O_t (>800 cm^{-1}) and bridging Nb–O_b–Nb (400–800 cm^{-1}) vibrations have different shifts. The terminal Nb–O_t vibration frequencies shift towards higher energies due to the protonation of polyniobate cluster anions.[15] However, the bridging Nb–O_b–Nb vibration frequencies of **2–4** have evident red shifts compared with that of the $[Nb_6O_{19}]^{8-}$ anion,[15,22] which may originate from the coordination of transition-metal cations with the bridging oxygen atoms of the polyniobates, thus impairing the Nb–O_b–Nb bonds, reducing the Nb–O_b–Nb bond force constant, and leading to a decrease in the Nb–O_b–Nb vibration frequency.

In Raman studies of $K_7HNb_6O_{19}\cdot 13H_2O$, **2**, and **3** in the solid state, bands corresponding to the terminal Nb–O_t and bridging Nb–O_b–Nb vibrations were observed, which display measurable shifts towards higher energies of the same bands in comparison to the nonprotonated $[Nb_6O_{19}]^{8-}$ cluster.[15] In particular, the characteristic vibrations of **2** and **3** were very similar, maybe due to their same fundamental building unit $[Nb_7O_{22}]^{9-}$. However, the solution Raman spectra of compounds **2** and **3** are almost entirely the same as that of the $K_7HNb_6O_{19}\cdot 13H_2O$ precursor. Three observed Raman bands at around 290, 485, and 890 cm^{-1} were polarized and can be assigned to the A_{1g} modes of the $[Nb_6O_{19}]^{8-}$ unit.[22] Another two depolarized Raman bands at about 165 and 805 cm^{-1} can be assigned to E_g or T_{2g} symmetry.[22] The similarity of the solid-state and solution Raman spectra demonstrates that the structure of the hexaniobate $[Nb_6O_{19}]^{8-}$ is retained in solution, which was previously confirmed by Tobias and Farrell et al.[22,23] Meanwhile, this result indicates that the cluster structures of **2** and **3** disassemble and retain the form of the $[Nb_6O_{19}]^{8-}$ unit in solution.

Magnetic measurements: The magnetic susceptibility of **3** was measured from 300 to 1.8 K at 0.1 kOe in the form of χ_M and $\chi_M T$ versus T as shown in Figure 8. At room temperature, the $\chi_M T$ is 7.55 emu K mol^{-1}, much less than the spin-only value of 9.92 emu K mol^{-1} for the Cu_{24} unit with $S_{Cu}=$ $^1/_2$ and assuming $g_{Cu}=2.1$. When the temperature is lowered, the $\chi_M T$ continuously decreases, reaching a minimum of 4.84 emu K mol^{-1} at 40 K; subsequently, it increases sharply to a maximum of 5.17 emu K mol^{-1} at 10 K and then falls to 3.84 emu K mol^{-1} at 1.8 K. The decreasing region of $\chi_M T$ indicates the presence of antiferromagnetic coupling interactions between the Cu^{II} ions with the spin-canting phenomenon. The maximum $\chi_M T$ value of 5.17 emu K mol^{-1} at 10 K corresponds to a spin ground state of $S\approx 3$, much less than

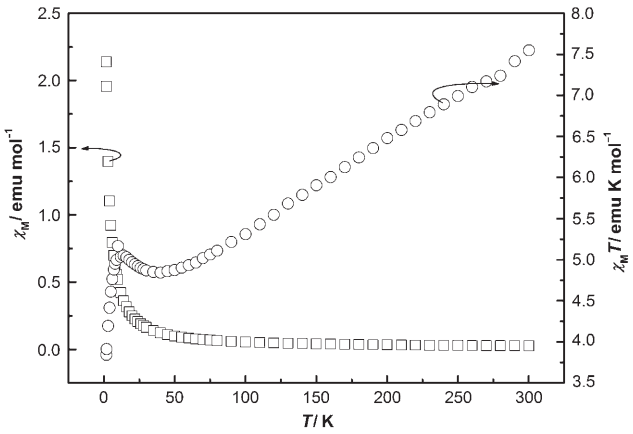

Figure 8. Temperature dependence of χ_M (□) and $\chi_M T$ (○) of **3** at an applied field (H) of 0.1 kOe in the range of 1.8–300 K.

the total spin value of 24 paramagnetic Cu^{II} ions, which is confirmed with variable-field magnetization measurements (Figure 9). After the maximum at 10 K, the spins are stabi-

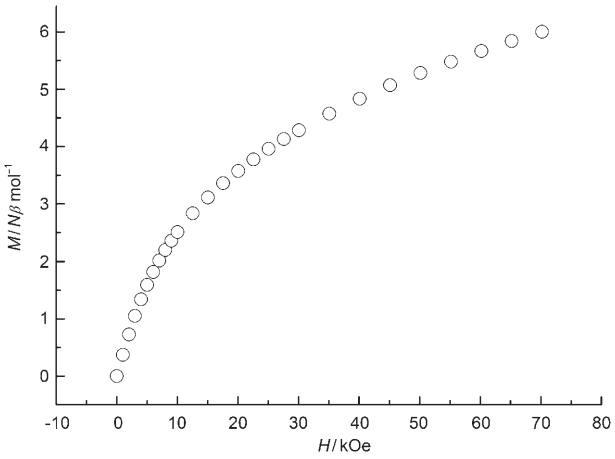

Figure 9. Field dependence of magnetization at 1.8 K for **3**.

lized by an applied field of 0.1 kOe, so a sharp decrease was observed due to Zeeman effects.

The plot of the reduced magnetization, $M/N\beta$ versus H/T, for **3** is shown in Figure 10. The eight isofield lines do not superimpose, indicting significant magnetic anisotropy (zero-field splitting) in the ground state for this Cu_{24} cluster. At low temperatures and high fields, the magnetization approaches a saturation state and $M=5.99\,N\beta$ mol^{-1} at 1.8 K and 7 T. In the crystal structure of **3**, all Cu^{II} ions take a slightly distorted square-planar geometry first to form 12 Cu_2 dimers, and then these dimers are connected by eight μ_4-O bridges (μ_4-OCu_3Na) leading to a Cu_{24} cluster (see Figure S20 in the Supporting Information). In dimers, the magnetic orbital is defined by $d(x^2-y^2)$ lying in the square plane and the Cu-O-Cu bridging angles range from 95 to 97.6°. It

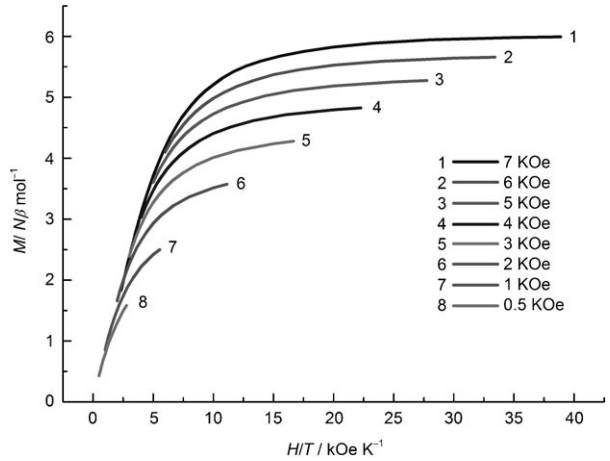

Figure 10. Plot of the reduced magnetization, $M/N\beta$ (N is Avogadro's number and β is the Bohr magneton) versus H/T at1.8 for **3**.

is well known that, for oxygen-bridged copper-containing complexes, the magnetic properties are usually regarded as strongly dependent on the Cu-O-Cu bridging angle if the bridging oxygen atoms coordinate to Cu^{II} ions via a $d(x^2-y^2)$ orbital and Cu_2O_2 is coplanar. When the Cu-O-Cu angle is smaller than 98°, the complex will show ferromagnetic characteristics,[24] and the smaller the angle is, the stronger the ferromagnetic coupling between Cu^{II} ions. So, the coupling interaction between Cu^{II} ions in the dimers is ferromagnetic. Furthermore, the observed magnetic properties in **3** actually result from the coupling among 12 dimers with $S=1$ bridged by eight μ_4-O atoms. The μ_4-O atoms adopt sp^3 hybridization, thus there is only one magnetic-exchange pathway via the sp^3 orbital of μ_4-O and the $d(x^2-y^2)$ orbitals of Cu^{II} ions among dimers. Their orbitals only partially overlap (Figure 11), so that μ_4-O mediates the weak coupling interaction among dimers. However, for a high-symmetry cluster such as **3**, it is difficult for all spins to align in a completely antiparallel state. So, it is suggested that spin canting may exist in this system. Because of the absence of an appropriate model for such a complicated magnetic coupling system, the coupling interaction between Cu^{II} ions was not estimated herein. Further magnetic investigations are under way.

Water content determination: To determine the amount of water, thermogravimetry (TGA) was performed on pure samples of compounds **2**–**4** (see Figures S24–S26 in the Supporting Information). The TGA curve of **2** (see Figure S24 in the Supporting Information) shows two distinct weight-loss events associated with the loss of lattice water and ethylenediamine ligands. The first weight loss of 9.0% between 20 and 205°C corresponds to 144 water molecules per molecular formula. The second weight loss of 11.8% up to 460°C is assigned to the decomposition of organic ethylenediamine groups. As for compounds **3** and **4**, the weight losses of 15.7% for **3** and 11.0% for **4** between 20 and 250°C correspond to around 106 and 73.5 lattice water molecules per molecular formula in **3** and **4**, respectively. These results agree well with the structural determination of **2**–**4**.

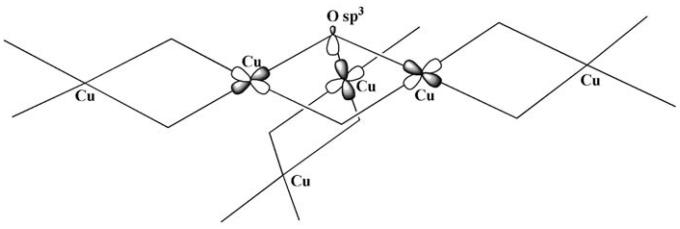

Figure 11. Magnetic orbital between μ_4-O and the neighboring Cu^{II} ions in **3**.

Conclusion

We have successfully synthesized a series of new copper(II)-participating polyniobate clusters under basic conditions. Compound **2** reveals the first 3D extended structure based on dimeric $[(\{KNb_{24}O_{72}H_{10.25}\}\{Cu(en)_2\})_2\{Cu_3(en)_3(H_2O)_3\}\{Na_{1.5}Cu_{1.5}(H_2O)_8\}]^{11-}$ building blocks with capsule cavities hosting the Lindqvist $[H_2Nb_6O_{19}]^{6-}$ anions. The unprecedented polyniobate clusters $[H_{23}NaO_8Cu_{24}(Nb_7O_{22})_8]^{16-}$ in **3** and $[H_9Cu_{25.5}O_8(Nb_7O_{22})_8]^{28-}$ in **4** represent a novel cube-shaped framework built from $[Nb_7O_{22}]^{9-}$ fundamental building blocks and copper bridges. Powder X-ray diffraction confirms that the bulk samples of these compounds are pure. Raman spectra studies of **2** and **3** reveal that the solid-state structures of these polyniobate cluster anions disassemble and exist in the form of the $[Nb_6O_{19}]^{8-}$ unit in solution. Magnetic susceptibility measurement of **3** shows the antiferromagnetic coupling interactions between Cu^{II} ions with the spin-canting phenomenon. The successful preparation of these polyniobates provides a feasible and effective synthetic route for searching and exploring novel polyniobate anion frameworks in synthetic chemistry and materials science.

Experimental Section

Materials and physical measurements: All reagents were used as purchased without further purification. $K_7HNb_6O_{19}\cdot 13H_2O$ was synthesized according to reference [20]. $Na_7HNb_6O_{19}\cdot 15H_2O$ was prepared according to the method in reference [21]. Other reagents were purchased commercially and used without further purification. Raman spectra of $K_7HNb_6O_{19}\cdot 13H_2O$, solid state: $\tilde{\nu}=216$ (s), 284 (s), 467 (m), 534 (s), 827 (s), 852 (m), 898 cm^{-1} (vs); solution spectra: $\tilde{\nu}=164$ (s), 296 (m), 482 (s), 803 (s), 885 cm^{-1} (m).

Preparation

Synthesis of 1: Ethylenediamine (en) was added dropwise to a stirred solution of $Cu(OOCCH_3)_2\cdot H_2O$ (0.6 g, 3.0 mmol) dissolved in 25 mL water, until the pH value of the solution was adjusted to 10–11. Then, the blue-violet solution was added dropwise to a stirred aqueous solution (50 mL) containing $Na_7HNb_6O_{19}\cdot 15H_2O$ (1.3 g, 1.0 mmol). Finally, the resulting mixture was stirred for 7 h, and was filtered and left to evaporate slowly at ambient temperature. After a week, blue-violet crystals of **1** were obtained. Yield: 0.53 g (51% based on $Na_7HNb_6O_{19}\cdot 15H_2O$); IR (KBr disks): $\tilde{\nu}=868$ (m), 832 (s), 741 (w), 703 (s), 662 (w-m), 645 (w-m), 525 cm^{-1} (s); elemental analysis calcd (%) for $C_{21}H_{168}C_{18}Cu_4N_{21}Nb_{48}O_{162}$: C 3.04, H 2.04, N 3.54; found: C 3.04, H 2.19, N 3.44.

Synthesis of 2: Ethylenediamine was added dropwise to a stirred solution of $Cu(OOCCH_3)_2{\cdot}H_2O$ (0.6 g, 3.0 mmol) dissolved in 25 mL water, until the pH value of the solution was adjusted to 10–11. Then, the blue-violet solution was added dropwise to a stirred aqueous solution (50 mL) containing $K_7HNb_6O_{19}{\cdot}13H_2O$ (1.37 g, 1.0 mmol) and $NaOOCCH_3$ (0.58 g, 7.0 mmol). Finally, the resulting mixture was kept at 50–60 °C and stirred for 7 h, then filtered and left to evaporate slowly at ambient temperature. After a week, blue-violet crystals were obtained. Yield: 0.63 g (53 % based on $K_7HNb_6O_{19}{\cdot}13H_2O$); IR (KBr disks): $\tilde{\nu}$ = 869 (s), 724 (w), 646 (s), 524 (s), 487 cm^{-1} (m); Raman solid-state spectra: $\tilde{\nu}$ = 156 (s), 213 (s), 285 (s), 477 (m), 534 (s), 556 (s), 777 (m), 813 (m), 863 (m), 898 cm^{-1} (vs); solution spectra: $\tilde{\nu}$ = 162 (s), 298 (m), 487 (s), 803 (s), 895 cm^{-1} (m); elemental analysis calcd (%) for $C_{114}H_{737.5}Cu_{37.5}K_6N_{114}Na_{4.5}Nb_{147}O_{551}$: C 4.74, H 2.57, N 5.52, K 0.81, Na 0.36, Cu 8.24, Nb 47.25; found: C 4.69, H 2.61, N 5.49, K 0.84, Na 0.32, Cu 8.43, Nb 47.69.

Synthesis of 3: An aqueous solution of $AgNO_3$ (0.01 mol L^{-1}, 2 mL) was added slowly to a stirred solution of $Na_7HNb_6O_{19}{\cdot}15H_2O$ (0.65 g, ≈0.5 mmol) in H_2O (25 mL) and a white precipitate was formed. A solution of $CuCl_2{\cdot}2H_2O$ (0.13 g, 1.25 mmol) in H_2O (5 mL) was added. The resulting dark-green mixture was heated at 77 °C for 5 h, then filtered and the filtrate was allowed to evaporate slowly at ambient temperature. After several days, green crystals suitable for X-ray diffraction were obtained. Yield: 0.27 g (42 % based on $Na_7HNb_6O_{19}{\cdot}15H_2O$); IR (KBr disks): $\tilde{\nu}$ = 867 (s), 779 (m), 667 (s), 519 cm^{-1} (w-s); Raman solid-state spectra: $\tilde{\nu}$ = 163 (s), 213 (s), 284 (s), 549 (s), 777 (m), 820 (m), 869 (s), 913 cm^{-1} (vs); solution spectra: $\tilde{\nu}$ = 170 (s), 298 (m), 483 (s), 806 (s), 877 (m), 905 cm^{-1} (s); elemental analysis calcd (%) for $H_{235}Cu_{24}K_{12}Na_5Nb_{56}O_{290}$: K 3.85, Na 0.94, Cu 12.51, Nb 42.69; found: K 3.81, Na 0.97, Cu 12.47, Nb 42.68.

Synthesis of 4: A sample of $K_7HNb_6O_{19}{\cdot}13H_2O$ (0.69 g, 0.5 mmol) was dissolved in H_2O (20 mL), and an aqueous solution of $BaCl_2{\cdot}2H_2O$ (0.12 g, 0.5 mmol) was added slowly with stirring until the solution became a white emulsion. Then, a solution of $CuSO_4{\cdot}5H_2O$ (0.19 g, 0.75 mmol) in H_2O (10 mL) was added dropwise. The green mixture was adjusted to the desired pH 10–11 with aqueous 0.5 M NaOH and then heated at 80 °C for 3 h. The solution was cooled to room temperature and filtered. After standing for several days, dark-green single crystals suitable for X-ray diffraction were collected. Yield: 0.14 g (22 % based on $K_7HNb_6O_{19}{\cdot}13H_2O$); IR (KBr disks): $\tilde{\nu}$ = 876 (m), 835 (m), 779 (w), 668 (vs), 635 (m), 412 cm^{-1} (vs); elemental analysis calcd (%) for $H_{156}Cu_{25.5}K_{16}Na_{12}Nb_{56}O_{257.5}$: K 5.21, Na 2.30, Cu 13.50, Nb 43.35; found: K 4.97, Na 2.45, Cu 13.17, Nb 43.68.

X-ray crystallographic studies of the compounds: X-ray intensity data of **1**, **3**, and **4** were collected on a Rigaku RAXIS-IV image-plate area detector, whilst data for **2** were collected on a Bruker CCD Apex-2 diffractometer by using graphite monochromated $Mo_{K\alpha}$ radiation (λ = 0.71073 Å). Lorentz polarization and empirical absorption corrections were empirically applied. Niobium and copper atoms were located by direct methods and other non-hydrogen atoms were found by successive differential Fourier syntheses. The structures were solved by direct methods and refined by using full-matrix least-squares on F^2. All calculations were performed with the SHELXL-97 program package.[25] All atoms except oxygen atoms were refined anisotropically. Hydrogen atoms were not included in the refinements. A summary of crystal data and structure refinement for compounds **1**–**4** is listed in Table 1.

CCDC-231468 (**1**) and CCDC-627110 (**2**) contain the supplementary crystallographic data for this paper. These data can be obtained free of charge from the Cambridge Crystallographic Data Centre via www.ccdc.cam.ac.uk/data_request/cif. Further details of the crystal structure investigation(s) may be obtained from the Fachinformationszentrum Karlsruhe, 76344 Eggenstein-Leopoldshafen, Germany (fax: (+49) 7247-808-666; e-mail: crysdata@fiz-karlsruhe.de) on quoting the depository number CSD-415045 (**3**) and CSD-417652 (**4**).

Physical measurements: X-ray powder diffraction was carried out with a Philips X-Pert Pro MPD diffractometer in Bragg–Brentano geometry with Ni-filtered $Cu_{K\alpha}$ radiation. IR spectra of samples were recorded on KBr disks with a Nicolet 170 SXFT-IR spectrometer in the range of 4000–400 cm^{-1}. Raman measurements were performed by means of a LabRam HR800 UV spectrometer; a He–Cd laser with a wavelength of 514 nm was used for excitation in the solid state and in solution. C, H, and N elemental analyses were performed on a Perkin–Elmer 240C elemental analyzer. Inductively coupled plasma (ICP) analysis was performed on a Jarrel–Ash J-A1100 spectrometer. TGA was performed with a Perkin–Elmer 7 thermal analysis system under nitrogen flow with a heating rate of 10 °C min^{-1}. Magnetic susceptibility measurements for compound **3** were obtained by the use of a Quantum Design MPMS-XL7 SQUID magnetometer at a temperature ranging from 1.8 to 300 K. The dc measurements were collected from −70 to 70 kOe.

Acknowledgements

This work was supported by the National Natural Science Foundation of China, Program for New Century Excellent Talents in University of Henan Province.

[1] a) *Polyoxometalate Chemistry: From Topology via Self-Assembly to Applications* (Eds: M. P. Pope, A. Müller), Kluwer, Dordrecht, **2001**; b) *Polyoxometalate Molecular Science* (Eds: J. J. Borrás-Almener, E. Coronado, A. Müller, M. T. Pope), Kluwer, Dordrecht, **2003**; c) *Polyoxometalate: From Platonic Solids to Anti-Retroviral Activity* (Eds: M. T. Pope, A. Müller), Kluwer, Dordrecht, **1994** (with special reference to the article of R. Thouvenot, M. Michelon, A. Tézé, G. Hervé, pp. 177–190); d) C. L. Hill, *Comp. Coord. Chem. II* **2003**, 4, 679–759; e) N. Mizuno, M. Misono, *Chem. Rev.* **1998**, *98*, 199–217; f) A. Müller, C. Serain, *Acc. Chem. Res.* **2000**, *33*, 2–10.

[2] a) M. T. Pope, *Heteropoly and Isopoly Oxometalates*, Springer, Berlin, **1983**; b) M. T. Pope, A. Müller, *Angew. Chem.* **1991**, *103*, 56–70; *Angew. Chem. Int. Ed. Engl.* **1991**, *30*, 34–38; c) A. Müller, F. Peters, M. T. Pope, D. Gatteschi, *Chem. Rev.* **1998**, *98*, 239–271; d) A. Müller, S. Roy, *Coord. Chem. Rev.* **2003**, *245*, 153–166; e) T. Yamase, *Chem. Rev.* **1998**, *98*, 307–326; f) I. V. Kozhevnikov, *Chem. Rev.* **1998**, *98*, 171–198; g) P. Mialane, C. Duboc, J. Marrot, E. Rivière, A. Dolbecq, F. Sécheresse, *Chem. Eur. J.* **2006**, *12*, 1950–1959.

[3] a) C. L. Hill, *Angew. Chem.* **2004**, *116*, 406–408; *Angew. Chem. Int. Ed.* **2004**, *43*, 402–404; b) N. M. Okun, T. M. Anderson, C. L. Hill, *J. Am. Chem. Soc.* **2003**, *125*, 3194–3195; c) J. T. Rhule, C. L. Hill, D. A. Judd, *Chem. Rev.* **1998**, *98*, 327–358; d) P. Mialane, A. Dolbecq, J. Marrot, E. Rivière, F. Sécheresse, *Chem. Eur. J.* **2005**, *11*, 1771–1778; e) J. A. Bergwerff, L. G. A. van de Water, T. Visser, P. De Peinder, B. R. G. Leliveld, K. P. De Jong, B. M. Weckhuysen, *Chem. Eur. J.* **2005**, *11*, 4591–4601.

[4] a) A. Müller, E. Krichemeyer, H. Bögge, M. Schmidtmann, C. Beugholt, P. Kögerler, C. Lu, *Angew. Chem.* **1998**, *110*, 1278–1281; *Angew. Chem. Int. Ed.* **1998**, *37*, 1220–1223; b) A. Müller, S. Q. N. Shah, H. H. Bögge, M. Schmidtmann, *Nature* **1999**, *397*, 48–50; c) D. L. Long, E. Burkholder, L. Cronin, *Chem. Soc. Rev.* **2007**, *36*, 105–121; d) A. Müller, P. Kögerler, C. Kuhlmann, *Chem. Commun.* **1999**, 1347–1358; e) P. Gouzerh, R. Villaneau, R. Delmont, A. Proust, *Chem. Eur. J.* **2000**, *6*, 1184–1192; f) V. Artero, A. Proust, P. Herson, P. Gouzerh, *Chem. Eur. J.* **2001**, *7*, 3901–3910.

[5] a) Y. H. Guo, C. W. Hu, X. L. Wang, Y. H. Wang, E. B. Wang, *Chem. Mater.* **2001**, *13*, 4058–4064; b) C. D. Wu, C. Z. Lu, H. H. Zhuang, J. S. Huang, *J. Am. Chem. Soc.* **2002**, *124*, 3836–3837; c) H. Y. An, E. B. Wang, D. R. Xiao, Y. G. Li, Z. M. Su, L. Xu, *Angew. Chem.* **2006**, *118*, 918–922; *Angew. Chem. Int. Ed.* **2006**, *45*, 904–908; d) J. W. Chang, J. Zhang, S. T. Zheng, M. B. Zhang, G. Y. Yang, *Angew. Chem.* **2006**, *118*, 79–83; *Angew. Chem. Int. Ed.* **2006**, *45*, 73–77; e) A. Müller, L. Toma, H. Bögge, M. Henry, E. T. K. Haupt, A. Mix, F. L. Sousa, *Chem. Commun.* **2006**, 3396–3398; f) A. Müller, J. Meyer, E. Krickemeyer, C. Beugholt, H. Bögge, F. Peters, M. Schmidtmann, P. Kögerler, M. J. Koop, *Chem. Eur. J.* **1998**, *4*, 1000–1006.

[6] a) A. Müller, A. M. Todea, H. Bögge, J. van Slageren, M. Dressel, A. Stammler, M. Rusu, *Chem. Commun.* **2006**, 3066–3068; b) D. L. Long, O. Brucher, C. Streb, L. Cronin, *Dalton Trans.* **2006**, 2852–2860; c) U. Kortz, S. Isher, M. H. Dickman, D. Ravot, *Inorg. Chem.* **2000**, *39*, 2915–2922; d) L. Ruhlmann, J. Canny, R. Contant, R. Thouvenot, *Inorg. Chem.* **2002**, *41*, 2477–2488; e) J. Y. Niu, D. J. Guo, J. P. Wang, J. W. Zhao, *Cryst. Growth Des.* **2004**, *4*, 241–247; f) S. Bareyt, S. Piligkos, B. Hasenknopf, P. Gouzerh, E. Lacôte, S. Thorimbert, M. Malacria, *Angew. Chem.* **2003**, *115*, 3526–3528; *Angew. Chem. Int. Ed.* **2003**, *42*, 2404–2406.
[7] K. Wassermann, M. H. Dickman, M. T. Pope, *Angew. Chem.* **1997**, *109*, 1513–1516; *Angew. Chem. Int. Ed. Engl.* **1997**, *36*, 1445–1448.
[8] S. S. Mal, U. Kortz, *Angew. Chem.* **2005**, *117*, 3843–3846; *Angew. Chem. Int. Ed.* **2005**, *44*, 3777–3780.
[9] a) B. W. Dale, M. T. Pope, *J. Chem. Soc. Chem. Commun.* **1967**, *67*, 792; b) C. M. Flynn, Jr., G. D. Stucky, *Inorg. Chem.* **1969**, *8*, 335–344; c) M. F. P. Silva, A. M. V. Cavaleiro, J. D. P. DeJesus, *J. Coord. Chem.* **2000**, *50*, 141–144; d) B. W. Dale, J. M. Buckley, M. T. Pope, *J. Chem. Soc. A* **1969**, 301–304; e) T. Ozeki, T. Yamase, H. Naruke, Y. Sasaki, *Inorg. Chem.* **1994**, *33*, 409–410; f) T. Ozeki, T. Yamase, H. Naruke, Y. Sasaki, *Bull. Chem. Soc. Jpn.* **1994**, *67*, 3249–3253; g) A. V. Besserguenew, M. H. Dickman, M. T. Pope, *Inorg. Chem.* **2001**, *40*, 2582–2586.
[10] A. Goiffon, E. Philippot, M. Maurin, *Rev. Chim. Miner.* **1980**, *17*, 466–476.
[11] M. T. Pope, *Heteropoly and Isopoly Oxometalates*, Springer, New York, **1983**, p. 40.
[12] E. J. Graeber, B. Morosin, *Acta Crystallogr. Sect. B* **1977**, *33*, 2137–2143.
[13] a) M. Nyman, F. Bonhomme, T. M. Alam, M. A. Rodriguez, B. R. Cherry, J. L. Krumhansl, T. M. Nenoff, A. M. Sattler, *Science* **2002**, *297*, 996–998; b) M. Nyman, F. Bonhomme, T. M. Alam, J. B. Parise, G. M. B. Vaughan, *Angew. Chem.* **2004**, *116*, 2847–2852; *Angew. Chem. Int. Ed.* **2004**, *43*, 2787–2792; c) F. Bonhomme, J. P. Larentaos, T. M. Alam, E. J. Maginn, M. Nyman, *Inorg. Chem.* **2005**, *44*, 1774–1785.
[14] M. Nyman, A. J. Celestian, J. B. Parise, G. P. Holland, T. M. Alam, *Inorg. Chem.* **2006**, *45*, 1043–1052.
[15] R. P. Bontchev, M. Nyman, *Angew. Chem.* **2006**, *118*, 6822–6824; *Angew. Chem. Int. Ed.* **2006**, *45*, 6670–6672.
[16] M. Maekawa, Y. Ozava, A. Yagasaki, *Inorg. Chem.* **2006**, *45*, 9608–9609.
[17] a) M. H. Cjoamg, C. W. Williams, L. Soderholm, M. R. Antonio, *Eur. J. Inorg. Chem.* **2003**, *14*, 2663–2669; b) A. J. Russell, J. A. Berberich, G. F. Drevon, R. R. Koepsel, *Annu. Rev. Biomed. Eng.* **2003**, *5*, 1–27.
[18] I. D. Brown, D. Altermatt, *Acta Crystallogr. Sect. B* **1985**, *41*, 244–247.
[19] a) J. R. Black, M. Nyman, W. H. Casey, *J. Am. Chem. Soc.* **2006**, *128*, 14712–14720; b) A. Goiffon, R. Granger, C. Bockel, B. Spinner, *Rev. Chim. Miner.* **1973**, *10*, 487–502.
[20] M. Filowitz, R. K. C. Ho, W. G. Klemperer, W. Shum, *Inorg. Chem.* **1979**, *18*, 93–103.
[21] C. M. Flynn, Jr., G. D. Stucky, *Inorg. Chem.* **1969**, *8*, 178–180.
[22] F. J. Farrell, V. A. Maroni, T. G. Spiro, *Inorg. Chem.* **1969**, *8*, 2638–2642.
[23] R. S. Tobias, *Can. J. Chem.* **1965**, *43*, 1222–1225.
[24] E. Ruiz, P. Alemany, S. Alvarez, J. Cano, *J. Am. Chem. Soc.* **1997**, *119*, 1297–1303.
[25] a) G. M. Sheldrick, SHELXL 97, Version 5.1, Program for Crystal Structure Solution and Refinement. University of Göttingen (Germany), **1997**; b) G. M. Sheldrick, SADABS, Program for Empirical Absorption Correction of Area Detector Data, University of Göttingen (Germany), **1996**.

Received: April 23, 2007
Published online: July 24, 2007

